Transport upscaling in highly heterogeneous alluvial aquifers and the prediction of tracer dispersion at the Macrodispersion Experiment (MADE) site

Marco Dentz, Alessandro Comolli, and Vivien Hakoun*
Spanish National Research Council (IDAEA-CSIC), Barcelona, Spain

We present an upscaled model to predict the plume evolution in highly heterogeneous alluvial aquifers. The model is parameterized exclusively by the mean, variance and correlation length of the logarithm of hydraulic conductivity, porosity and the mean hydraulic gradient. It can be conditioned on the tracer and conductivity data at the injection region. The model predicts the evolution of the longitudinal mass distribution observed at the MADE site, which is characterized by strongly non-Gaussian plume shapes with a localized peak and pronounced forward tail. The proposed model explains these features by the conductivity heterogeneity at the injection region, and tracer propagation due to a broad distribution of spatially persistent Eulerian flow speeds.

I. INTRODUCTION

The upscaling and prediction of tracer transport in highly heterogeneous porous and fractured media is of central concern in a broad range of subsurface applications from groundwater management to underground gas and waste storage. This task is challenging due to strong spatial variability in hydraulic conductivity values encountered in geological media [1].

Spatial variability in hydraulic conductivity induces spatial fluctuations in the flow and transport velocities, whose impact on large scale tracer migration has been quantified in terms of macrodispersion coefficients [2, 3]. For moderately heterogeneous media, [2] used a stochastic modeling approach [4–6] to express the longitudinal macrodispersion coefficients in terms of the mean flow velocity, and the correlation length and variance of the logarithm of hydraulic conductivity. This expression is a central results for hydrogeological prediction because it allows to forecast macroscopic transport features based on transport independent observables.

However, spatial heterogeneity gives rise to transport behaviors that can be very different from the ones predicted by advection-dispersion models characterized by constant macrodispersion coefficients. For pointlike solute injections, the latter predicts Gaussian shaped tracer plumes and breakthrough curves, while observed distributions are typically found to be non-Gaussian [7–11]. This is the case for the tracer plumes observed during the macrodispersion experiments conducted in the alluvial aquifer underlying the Columbus Air Force Base in northeastern Mississippi [7, 12]. Spatial tracer distributions are characterized by strongly non-Gaussian shapes characterized by a slowly moving peak and a pronounced forward tail. These and other observations of anomalous solute dispersion have spurred the development of non-Fickian transport theories [13–16]. Those include multirate mass transfer approaches [17, 18], continuous time random walks [13, 19], fractional advection-dispersion models [20, 21], time-domain random walks [22, 23], and space-time non-local advection-dispersion equations [24, 25]. While all of these approaches provide dynamic frameworks to model non-Gaussian large scale transport features, their parameterization in terms of transport independent parameters and thus their predictive power remain open questions.

The migration of the tracer plume at the MADE site was modeled by [26] with the CTRW approach based on an empirical distribution of transition length and times, which reflects a broad distribution of mass transfer time scales. [27] model the plume evolution using an MRMT model that considers rate limited mass transfer between a mobile domain with accelerating flow, and an immobile zone, which represents intragranular porosity, low permeability zones, dead end pores and surface sorption sites. These processes are lumped into into a capacity coefficient, a rate coefficient, a retardation coefficient, a velocity parameter and an acceleration parameter, which are estimated from the experimental data. [28] modeled the tracer plumes of the MADE-1 experiment using a fractal mobile-immobile model that accounts for both solute retention due to a broad distribution of mass transfer time scale, and preferential transport due to a broad distribution of mass transfer length scales. The characteristic exponents of the model are estimated from the experimental data. These modeling approaches propose a range of mass transfer processes and invoke broad distributions of mass transfer time scales and lengths in order to simulate the impact of medium and flow heterogeneity on large scale transport. A key question in order to constrain such models refers to the actual local scale mechanisms that cause non-Fickian large scale transport.

* E-mail: marco.dentz@csic.es

A series of works [29–31] have shown that a local scale advection-dispersion model based on the detailed knowledge of the spatial distribution of hydraulic conductivity allows reproducing the tracer plumes observed at the MADE site. This implies that the observed tracer plumes can indeed be understood from the spatial variability of hydraulic conductivity and thus advective heterogeneity. The question arising from this observation is whether non-Fickian transport in strongly heterogeneous media can be predicted based only on a few geostatistical medium characteristics similar to the prediction of macrodispersion in moderately heterogeneous media. Along these lines, several authors [23, 32–34] investigated the relation between advective travel times and hydraulic conductivity, and the impact of broad distributions of the logarithm of hydraulic conductivity on non-Fickian transport. The stochastic multi-indicator approach of [23] was adapted in [35] to predict the plume evolution of the MADE-1 experiment based on analytical expressions for the advective travel times over rectangular inclusions.

In this paper, we adress the questions of upscaling and prediction of dispersion in highly heterogeneous alluvial aquifers based on a stochastic time domain random walk approach [36, 37]. This modeling framework propagates particles in space and time according to a velocity Markov model that is determined by the distribution of the Eulerian speed and correlation length. We discuss the parameterization of the model in terms of the medium and flow properties, and use it for the modeling and interpretation of the one-dimensional tracer profiles of the MADE-1 experiment.

II. UPSCALED TRANSPORT MODEL

We employ the stochastic time-domain random walk (TDRW) approach presented in [37] in order to built an upscaled model to predict the concentration evolution in highly heterogeneous alluvial aquifers, based on the statistical characteristics of the logarithm of hydraulic conductivity, porosity and the mean hydraulic gradient. We consider purely advective transport, which is a reasonable assumption given that the Péclet number at the MADE site is around 10^3 [35]. The method propagates solute particles at constant space increments whose duration is obtained from a Markov chain representation for the particle speed. In the following, we detail the model, its assumptions and parameterization.

Particle motion is quantified by the following stochastic evolution equations for the longitudinal particle position $x(s)$ and particle time $t(s)$,

$$\frac{dx(s)}{ds} = \chi^{-1}, \qquad \frac{dt(s)}{ds} = \frac{1}{v_\ell(s)} \tag{1}$$

where s is the distance along streamline, $v_\ell(s) > 0$ the particle speed and χ advective tortuosity. Advective tortuosity measures the ratio of streamline distance and average linear distance [37]. The particle speed $v_\ell(s)$ describes an ergodic and stationary Markov process characterized by the steady state distribution $p_v(v)$. The latter is a Lagrangian quantity, which, however, can be related to the distribution of Eulerian flow speed $p_e(v)$ via the flux-weighting relation [37, 39]

$$p_v(v) = \frac{v p_e(v)}{\langle v_e \rangle}. \tag{2}$$

The Eulerian velocity $\mathbf{v}_e(\mathbf{x})$ is given by the Darcy flux $\mathbf{q}(\mathbf{x})$ and porosity ϕ as $\mathbf{v}_e(\mathbf{x}) = \mathbf{q}(\mathbf{x})/\phi$. We assume the porosity is constant. The Darcy flux satisfies

$$\mathbf{q}(\mathbf{x}) = -K(\mathbf{x})\nabla h(\mathbf{x}), \qquad \nabla \cdot \mathbf{q}(\mathbf{x}) = 0, \tag{3}$$

where $K(\mathbf{x})$ is hydraulic conductivity and $h(\mathbf{x})$ hydraulic head. The Eulerian speed is $v_e(\mathbf{x}) = |\mathbf{v}_e(\mathbf{x})|$, and its distribution is, as introduced above, denoted by $p_e(v)$. Hydraulic conductivity is represented by a three-dimensional lognormally distributed spatial random field. The vertical correlation length $\ell_v \ll \ell_h$ is much smaller than the horizontal, which is typical for alluvial aquifers. We assume that the Eulerian speed can be approximated by

$$v_e(\mathbf{x}) = K(\mathbf{x})J/\phi, \tag{4}$$

where J is the magnitude of the mean hydraulic gradient. This relation is exact for stratified media [40] and a good approximation for media characterized by channel like structures. Furthermore, the advective tortuosity is set to $\chi = 1$. Based on (4), the Eulerian velocity distribution is given in terms of the distribution $p_k(k)$ of hydraulic conductivity as

$$p_e(v) = \frac{\phi p_k(v\phi/J)}{J}. \tag{5}$$

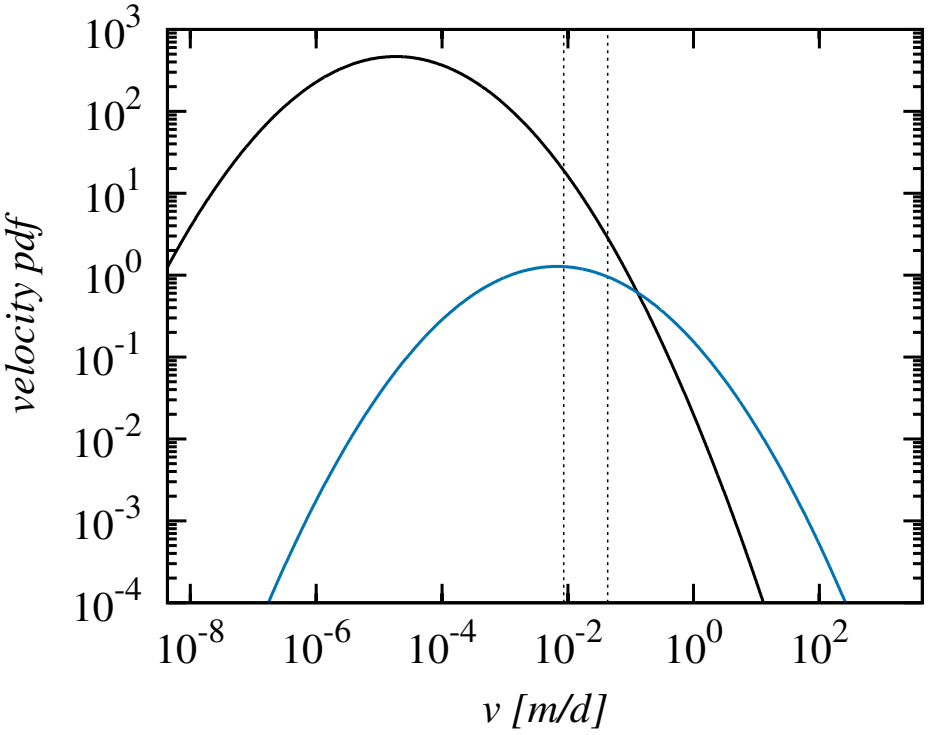

Figure 1. (Solid black line) Eulerian velocity distribution $p_e(v)$, (solid blue line) distribution of particle velocity $p_v(v)$. The initial velocities are sampled from $p_v(v)$ in the velocity range indicated by the vertical dashed lines.

The conductivity point distribution is lognormal, characterized by the mean $\overline{f} = \ln K_g$ and variance σ_f^2 of $f(\mathbf{x}) = \ln[K(\mathbf{x})]$,

$$p_k(k) = \exp\left(-[\ln(k) - \ln(K_g)]^2/2\sigma_f^2\right)/k\sqrt{2\pi\sigma_f^2}. \tag{6}$$

Thus, the Eulerian and Lagrangian speeds are also lognormally distributed and obtained from (6) through (5) and (2), respectively. This implies that the variances of both the logarithms of the Eulerian and Lagrangian speeds are equal to σ_f^2, the geometric mean of the Eulerian speed is $v_g = K_g J/\phi$, and the geometric mean of the particle speed is $v_g \exp(\sigma_f^2)$. Figure 1 illustrates the Eulerian and Lagrangian speed distributions corresponding to the lognormal conductivity distribution (6) for the parameters give in Table I.

In order to propagate the particle velocities $v_\ell(s)$ from their initial values $v_0 = v(0)$, we use an Ornstein-Uhlenbeck process for the normal score of $v_\ell(s)$ [36, 37]. The normal score $w(s)$ of $v_\ell(s)$ is here simply given by

$$w = \frac{\ln(v) - [\ln(v_g) + \sigma_f^2]}{\sigma_f}, \qquad\qquad v = v_g \exp(\sigma_f w + \sigma_f^2) \tag{7}$$

The normal score $w(s)$ evolves according to the Ornstein-Uhlenbeck process [41]

$$\frac{dw(s)}{ds} = -\ell_c^{-1} w(s) + \sqrt{2\ell_c^{-1}}\eta(s), \tag{8}$$

where $\eta(s)$ is a Gaussian white noise characterized by 0 mean and correlation $\langle \eta(s)\eta(s')\rangle = \delta(s-s')$. The steady state distribution of $w(s)$ is the unit Gaussian. The initial values $w(0)$ of the normal scores are obtained from $v(0)$ through the Smirnov transform (7). The initial velocity distribution is denoted by $p_0(v)$. For the correlation length ℓ_c of the normal score $w(s)$ we employ the same value as for the horizontal conductivity correlation length, which $\ell_c \approx \ell_h$.

Equations (1) together with the evolution equation for $v_\ell(s)$, describe the propagation of the particle position $x(s)$ and velocity $v_\ell(s)$ from the initial values $x(0)$, and $v(0)$, which are distributed according to $\rho(x)$, and $p_0(v)$. The initial value of time is $t(0) = 0$. The projected streamwise concentration profile $c(x,t)$ in this framework is obtained

Parameter	σ_f^2	K_g [m/s]	ℓ_h [m]	ℓ_v [m]	J [-]	ϕ
Value	5.9	6.7×10^{-6}	9.1	1.8	3.6×10^{-3}	0.31

Table I. Geostatistical and hydraulic parameters for the MADE site and MADE1 experiment according to Bohling *et al.* [38] and Boggs *et al.* [12].

by

$$c(x,t) = \langle \delta \left[x - s(t)/\chi \right] \rangle , \tag{9}$$

where $s(t) = \max[s|t(s) \leq t]$. The angular brackets denote the average over all particles. In the following, we use this upscaled transport model to predict the longitudinal plume evolution of the MADE-1 experiment. The numerical implementation of the upscaled model is detailed in the Appendix.

The upscaled model described above is fully defined by the hydraulic conductivity distribution $p_k(k)$, advective tortuosity χ, which here is set equal to 1, and the correlation length ℓ_c. We distinguish between these parameters, which determine the way the system is propagated, and the initial data for particle positions and velocities, which depend on the injection conditions and on the details of the heterogeneity distribution at the injection region.

III. PREDICTION OF DISPERSION AT THE MADE SITE

We apply the upscaled transport model presented in the previous section, for the prediction of the streamwise tracer profiles of the MADE-1 experiment. In order to parameterize the model, we rely on description of the experimental conditions in [12] and [7] and the geostatistical characterization of the hydraulic conductivity field given in [38]. Thus, the medium porosity and the magnitude of the mean hydraulic gradient are set equal to $\phi = 0.31$ and $J = 3.6 \times 10^{-3}$ [7, 12, 35]. [38] obtain for the geometric mean conductivity the value $K_g = 6.7 \times 10^{-6}$ m/s, for the variance of the logarithm of conductivity $\sigma_f^2 = 5.9$ and for the horizontal and vertical correlation length $\ell_h = 9.1$ m and $\ell_v = 1.8$ m. These values are summarized in Table I. As pointed out at the end of the previous section, these parameter values determine the propagator of the upscaled transport model. In order to predict the plume evolution, we need both the propagator, and the the initial conditions, this means here, the initial particle positions, i.e., initial tracer distribution, and initial particle speed distribution.

As described in [12], tracer was injected into five 5.2-cm-diameter injection wells separated by 1 m in a linear array perpendicular to the mean flow direction. This justifies the use of a pointlike initial particle distribution, localized at the origin at $x = 0$,

$$\rho(x) = \delta(x). \tag{10}$$

On the other hand, the tracer was injected at constant rate with 10.07 m^2 of groundwater during 48.5 h. This would imply a uniform initial plume of an extension of $\ell_0 = 2.68$ m centered at $x = 0$. In the following, we employ for the sake of simplicity the pointlike initial condition (10). However, as shown in the Appendix, there is virtually no difference between the predictions using the pointlike or uniform initial plumes. This demonstrates the robustness of the model and of the actual flow and transport system.

Regarding the initial velocity distribution $p_0(v)$, we note that [12] estimated the typical hydraulic conductivity value in the injection region to be of the order of 10^{-5} m/s, which corresponds to an advective speed of approximately 10^{-7} m/s or 10^{-2} m/d. This is also consistent with the experimental observation that the peak moved about 5 m in 500 days [7]. Thus, we consider a velocity window of 10^{-7} m/s $< v < 5 \times 10^{-7}$ m/s, as illustrated in Figure 1. As pointed out in [12] and [35], more mass entered in the high than in the low conductivity zones, which implies that the initial mass distribution is approximately flux-weighted. The flux-weighted Eulerian speed distribution is equal to $p_v(v)$, see Eq. (2). Thus, we set $p_0(v)$ equal to

$$p_0(v) = p_v(v) \Big/ \int_{v_\ell}^{v_u} dv' p_v(v) \tag{11}$$

for $v_\ell < v \leq v_u$ and 0 else, where $v_\ell = 10^{-7}$ m/s and $v_u = 5 \times 10^{-7}$ m/s.

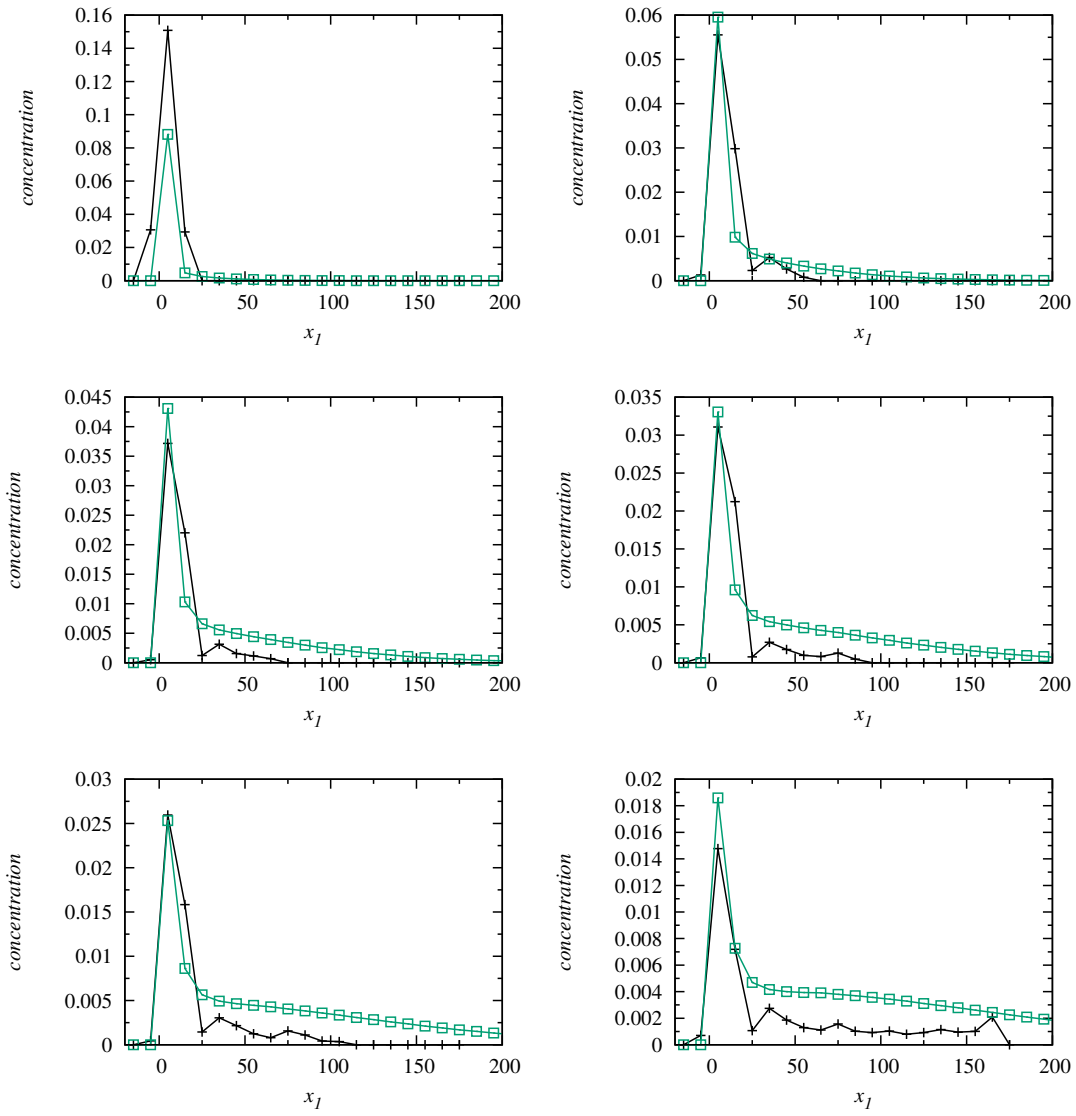

Figure 2. Concentration profiles from the (black crosses) MADE data and the upscaled model for an averaging window of (green squares) $\Delta x = 10$ m at times (top left to bottom right) $t = 49$ d, 126 d, 202 d, 279 d, 370 d and 503 d using a pointlike initial distribution.

A. Longitudinal tracer profiles

Figure 2 shows the experimental and predicted longitudinal concentration distributions. As explained in [7], concentration values between sampling wells were linearly interpolated. The data displayed in Figure 2 was obtained by vertical and transverse integration of the concentration field, as well as longitudinal averaging over a window of $\Delta x = 10$ m. The bin centers are located at $x_i = -15$ m $+ i10$ m with $i = 0, \ldots, 19$. Concentration values are normalized by the initial mass. The longitudinal concentration distribution is shown at 6 snapshots at times $t = 49, 126, 202, 279, 370$ a d 503 days. The tracer distributions predicted from the upscaled model are presented in the same way. For comparison, we show in Figure 3 the tracer distributions with an averaging window of $\Delta x = 10^{-1}$ m. We refer to the latter as the fine scale data.

We first notice that the experimental data does not integrate to 1. In fact the are under the longitudinal profiles integrates to $2.06, 0.99, 0.68, 0.62, 0.54$ and 0.43 for the six snapshots at increasing time [35]. As discussed in Adams and Gelhar [7] and Fiori *et al.* [35], the mass loss for $t > 49$ days can mainly be attributed to the downstream plume truncation and low density of sampling points at distances larger than 20 m downstream from the injection region. This is supported by the results of the upscaled model, which predicts a significant downstream tailing beyond the

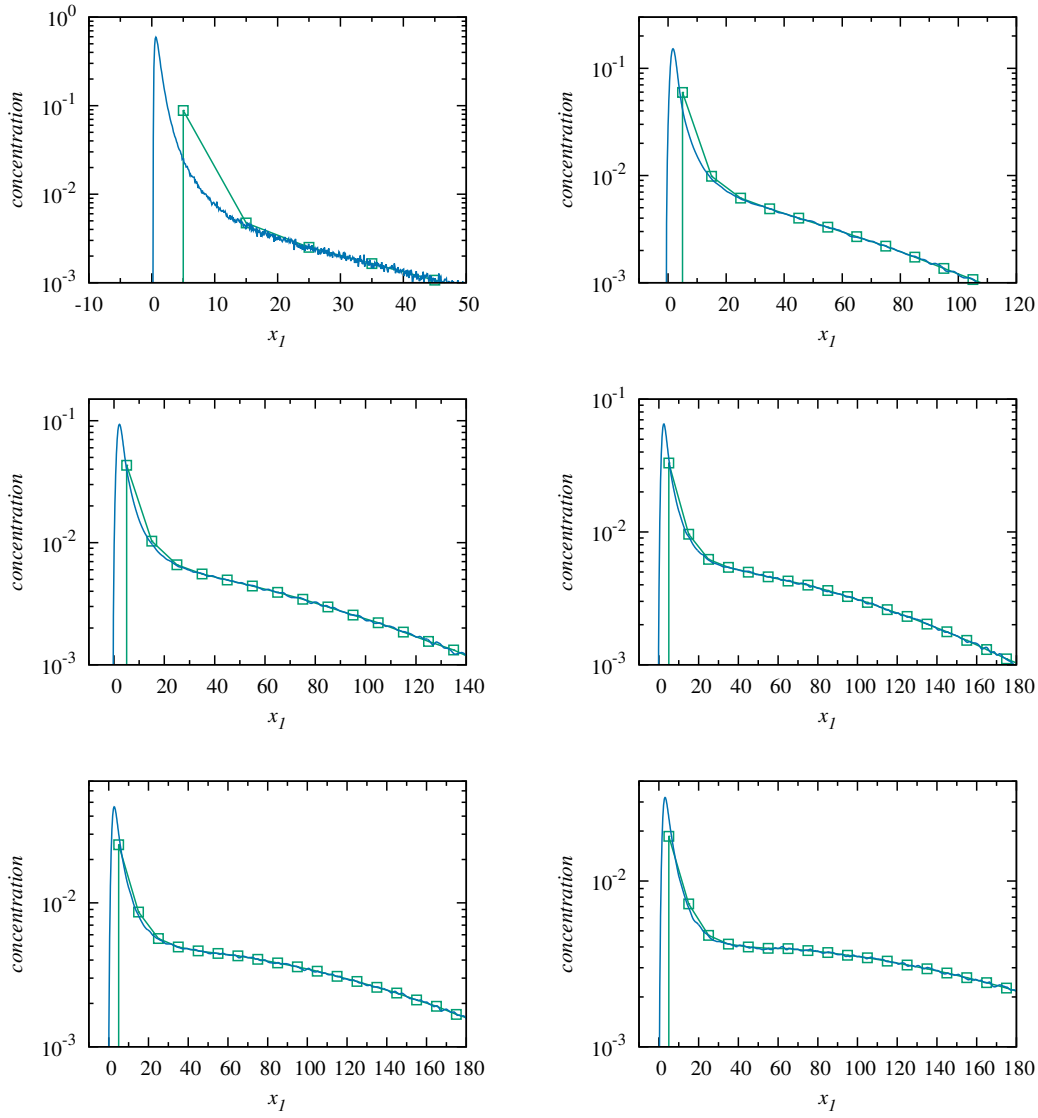

Figure 3. Concentration profiles from the (black crosses) MADE data and the upscaled model for an averaging window of (green squares) $\Delta x = 10$ m and (dash dotted blue line) $\Delta x = 10^{-1}$ m at times (top left to bottom right) $t = 49$ d, 126 d, 202 d, 279 d, 370 d and 503 d using a pointlike initial distribution.

maximum sampling distance at 180 m. As discussed in [7], the excess mass at $t = 49$ d may be due to the fact that the spatial integration used to estimate the mass recovery assumes a uniform tracer concentration while the multilevel samplers may sample mainly from localized high concentration regions. This interpretation is supported by the fine scale data, which predicts a sharply peaked tracer distribution at $t = 49$ days.

The tracer distribution in the upscaled model is by default normalized to 1 and predicts the overall shape of the observed tracer distributions with the localized peak at $x = 5$ m and strong downstream tailing. Like Fiori *et al.* [35], we tend to attribute differences in the tail of the experimental and predicted concentrations to the low density of samplers at distances large than 20 m downstream from the injection region. This would explain that the values are higher in the predicted than in the experimental tail concentrations. The stochastic TDRW model captures the retention of tracer mass in the injection region by conditioning on the initial velocity through (11), and fast tracer motion through particle transitions into spatially persistent fast velocity channels.

The comparison between the coarse and fine scale model predictions shows that the averaging window of $\Delta x = 10$ m introduces an artificial broadening of the peak due to oversmoothing, while the tail concentrations are nearly identical. With increasing time, as the peak width increases due to hydrodynamic dispersion, the differences between the coarse and fine scale models decrease.

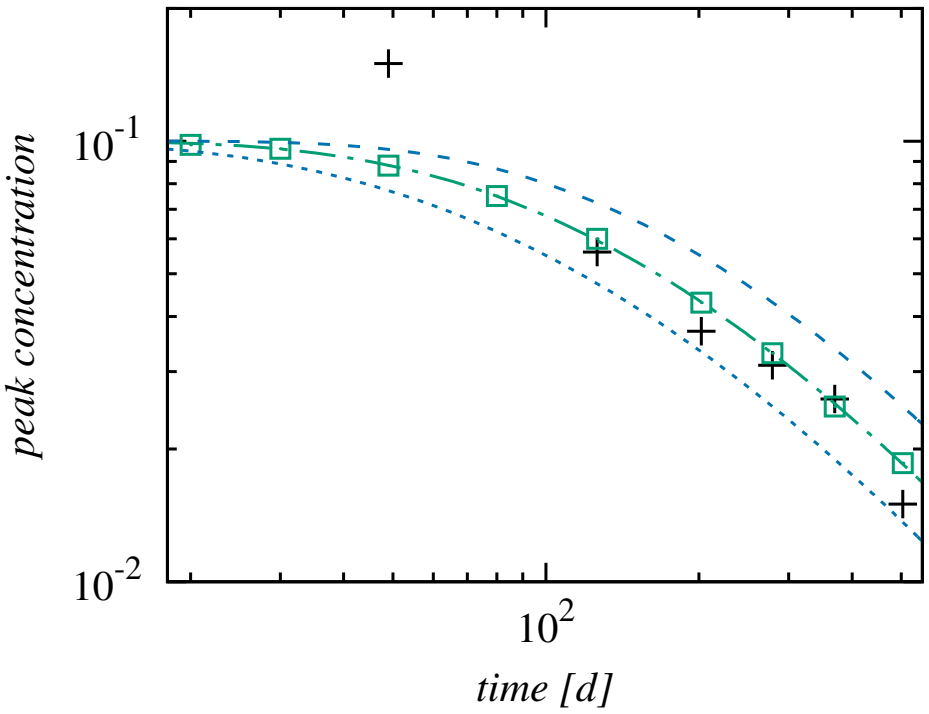

Figure 4. Maximum concentrations versus times from the (black crosses) MADE data, and (green squares) the prediction from the upscaled model with $\Delta x = 10$ m. The dashed-dotted line denotes cumulative distribution of residence times (12) obtained from the upscaled model for $p_0(v)$ given by (11) with $v_\ell = 10^{-7}$ m/s and $v_u = 5 \times 10^{-7}$ m/s. The dashed and dotted lines denote the residence time distribution for $v_u = 2.5 \times 10^{-7}$ m/s and $v_u = 10^{-6}$ m/s with $v_\ell = 10^{-7}$ m/s.

B. Peak concentrations

The concentration peak is localized at all snapshots at $x = 5$ m, which indicates that it does not move beyond the averaging window between $x = 0$ m and 10 m. This is supported by the fine scale prediction. The upscaled model predicts peak heights and widths that are qualitatively and quantitatively similar to the experimental observations. The peak concentrations from the experimental data, and the corresponding model predictions are displayed in Figure 4. The upscaled model predicts the overall decay of the peak concentration. The decay behavior in the localized peak is in fact a measure for the residence time in the injection region. The mass $m_0(t)$ remaining in the region between 0 m and 10 m is equal to the probability that the residence time τ_0 of a particle is larger than t,

$$m_0(t) = \int_t^\infty dt' \psi_0(t'), \tag{12}$$

where $\psi_0(t)$ denotes the residence time distribution. As long as the mass in the injection region of size Δx is larger than the mass in all other bins, the peak concentration is equal to $c_0(t) = m_0(t)/\Delta x$. Figure 4 shows the evolution of $c_0(t)$ from experimental data and model prediction compared to the cumulative distribution of residence times in the injection bin obtained from the upscaled model. In order to highlight the impact of the conductivity in the injection regions, we plot the decay of the maximum concentration for $p_0(v)$ given by (11) with $v_u = 10^{-6}$ m/s and $v_u = 2.5 \times 10^{-7}$ m/s. The former underestimates the observed maximum concentrations because higher velocities together with persistence over the distance ℓ_c leads to a faster tracer release from the injection domain. The latter overestimates the maximum concentration because of stronger tracer retention at the injection region. Nevertheless, both cases display qualitatively the same non-Gaussian behavior for the tracer profiles (not shown) as the ones in Figure 2. This shows the robustness of the salient non-Gaussian transport features, and emphasizes the importance of accounting for the the conductivity in the source zone. Furthermore, this observation implies that the conductivity heterogeneity may be inferred from the evolution of the maximum concentration in the injection area.

IV. CONCLUSIONS

We have presented a particle based model for transport in alluvial aquifers that is parameterized in terms of the statistical characteristics of hydraulic conductivity. The model is based on a Markov processes for equidistant particle velocities, and assumes that the Eulerian flow speed can be expressed in terms of hydraulic conductivity, the mean hydraulic gradient, and porosity. This assumption yields an efficient predictive model for tracer transport in heterogeneous media. We use this upscaled model to predict the evolution of the tracer plume of the MADE-1 experiment, which is characterized by strongly non-Gaussian shapes. Relatively low conductivity in the source zone leads to slow peak movement of only a few meters over the duration of 500 days, while part of the tracer moves fast in high conductivity channels, which gives rise to a pronounced forward tail. These behaviors are captured by the upscaled model through conditioning on the conductivity data in the injection region, and tracer propagation due to spatially persistent and broadly distributed Eulerian flow speeds. The model predicts a higher concentration in the forward tail than obtained in the experiment. However, the concentration data in the forward tail is less reliable than the concentration around the peak due to the sparseness of the network of monitoring wells beyond 20 m downstream of the injection array. The evolution of the mass contained within 10 m of the injection point is well predicted by the proposed model, which relates it to the conductivity distribution in the source region. Thus, the upscaled model seems to capture the salient heterogeneity mechanisms, and their impact on non-Fickian large scale dispersion. It is predictive, and highlights the importance of conditioning on the conductivity data in the source region.

ACKNOWLEDGMENTS

The authors acknowledge the financial support of the European Research Council through the project MHetScale (Grant agreement No. 617511). The experimental data was published originally in [7]. The model data can be obtained by numerically solving the upscaled model following the model implementation detailed in the Appendix.

[1] J. Bear, *Dynamics of Fuids in Porous Media* (American Elsevier, New York, 1972).
[2] L. W. Gelhar and C. L. Axness, Water Resour. Res. **19**, 161 (1983).
[3] G. Dagan, J. Fluid Mech. **145**, 151 (1984).
[4] G. Dagan, *Flow and transport in porous formations* (Springer, New York, 1989).
[5] L. W. Gelhar, *Stochastic subsurface hydrology* (Prentice Hall, 1993).
[6] Y. Rubin, *Applied stochastic hydrogeology* (Oxford University Press, New York, 2003).
[7] E. E. Adams and L. W. Gelhar, Water Resour. Res. **28**, 3293 (1992).
[8] M. Levy and B. Berkowitz, Journal of Contaminant Hydrology **64**, 203 (2003).
[9] R. Haggerty, S. A. McKenna, and L. C. Meigs, Water Resour. Res. **36**, 3467 (2000).
[10] C. Zheng, M. Bianchi, and S. M. Gorelick, Groundwater **49**, 649 (2011).
[11] P. K. Kang, T. Le Borgne, M. Dentz, O. Bour, and R. Juanes, Water Resour. Res. **51**, 940 (2015).
[12] J. M. Boggs, S. C. Young, L. M. Beard, L. W. Gelhar, K. R. Rehfeldt, and E. E. Adams, Water Resour. Res. **28**, 3281 (1992).
[13] B. Berkowitz, A. Cortis, M. Dentz, and H. Scher, Rev. Geophys. **44**, RG2003 (2006).
[14] S. P. Neuman and D. M. Tartakovsky, Adv. Water Resour. **32**, 670 (2008).
[15] M. Dentz, T. Le Borgne, A. Englert, and B. Bijeljic, J. Cont. Hydrol. **120-121**, 1 (2011).
[16] B. Noetinger, D. Roubinet, A. Russian, T. Le Borgne, F. Delay, M. Dentz, J.-R. De Dreuzy, and P. Gouze, Transport in Porous Media , 1 (2016).
[17] R. Haggerty and S. M. Gorelick, Water Resour. Res. **31**, 2383 (1995).
[18] J. Carrera, X. Sánchez-Vila, I. Benet, A. Medina, G. Galarza, and J. Guimerà, Hydrogeology Journal **6**, 178 (1998).
[19] B. Berkowitz and H. Scher, Phys. Rev. Lett. **79**, 4038 (1997).
[20] D. A. Benson, S. W. Wheatcraft, and M. M. Meerschaert, Water Resources Research **36**, 1403 (2000).
[21] J. H. Cushman and T. R. Ginn, Water Resour. Res. **36**, 3763 (2000).
[22] V. Cvetkovic, H. Cheng, and X.-H. Wen, Water Resour. Res. **32**, 1671 (1996).
[23] A. Fiori, I. Jankovic, G. Dagan, and V. Cvetkovic, Water Resour. Res. **43**, W09407 (2007).
[24] J. Cushman and T. Ginn, Transp. Porous Media **13**, 123 (1993).
[25] S. P. Neuman, Water Resour. Res **29**, 633 (1993).
[26] B. Berkowitz and H. Scher, Phys. Rev. E **57**, 5858 (1998).
[27] C. Harvey and S. M. Gorelick, Water Resources Research **36**, 637 (2000).
[28] R. Schumer, D. A. Benson, M. M. Meerschaert, and B. Bauemer, Water Resour Res **39(10)**, 1296 (2003).
[29] H. C. Barlebo, M. C. Hill, and D. Rosbjerg, Water Resour. Res. **40**, W04211 (2004).
[30] P. Salamon, D. Fernàndez-Garcia, and J. J. Gómez-Hernández, Water Resour. Res. **43**, W08404 (2007).

[31] M. Dogan, R. L. Van Dam, G. Liu, M. M. Meerschaert, J. J. Butler Jr., G. C. Bohling, D. A. Benson, and D. W. Hyndman, Geophys. Res. Lett. **41**, 7560 (2016).
[32] V. Cvetkovic, A. Fiori, and G. Dagan, Water Resources Research **50**, 5759 (2014).
[33] Y. Edery, A. Guadagnini, H. Scher, and B. Berkowitz, Water Resour Res **50 (2)**, 1490 (2014).
[34] A. Tyukhova, M. Dentz, W. Kinzelbach, and M. Willmann, Physical Review Fluids **1**, 074002 (2016).
[35] A. Fiori, G. Dagan, I. Jankovic, and A. Zarlenga, Water Resources Research **49**, 2497 (2013).
[36] V. Hakoun, A. Comolli, and M. Dentz, Water Resour. Res. **55**, 10.1029/2018WR023810 (2019).
[37] A. Comolli, V. Hakoun, and M. Dentz, Water Resour. Res. **accepted** (2019).
[38] G. C. Bohling, G. Liu, P. Dietrich, and J. J. Butler, Water Resources Research **52**, 8970 (2016).
[39] M. Dentz, P. K. Kang, A. Comolli, T. Le Borgne, and D. R. Lester, Physical Review Fluids **1**, 074004 (2016).
[40] M. Matheron and G. de Marsily, Water Resour. Res. **16**, 901 (1980).
[41] C. W. Gardiner, Applied Optics **25**, 3145 (1986).

Appendix A: Numerical model implementation

In the following, we outline the basic steps of the numerical implementation of the stochastic time domain random walks model. First, we note that the steady state velocity distribution $p_v(v)$ is given by the lognormal distribution

$$p_v(v) = \frac{\exp\left(-[\ln(v) - \ln(v_g) - \sigma_f^2]^2/2\sigma_f^2\right)}{v\sqrt{2\pi\sigma_f^2}}, \tag{A1}$$

Step 1: Initialization Initial particle velocities $v(0)$ are sampled from the uniform distribution (11), particle positions $x(0)$ are chosed from the initial particle distribution $\rho(x)$.

Step 2: Propagation of normal scores The initial velocities $v(0)$ are then converted to the initial values $w(0)$ of the normal scores using the map (7). The normal scores $w(s)$ are propagated from their initial values $w(0)$ according to the Ornstein-Uhlenbeck process (8), which is discretized by using an Euler scheme. This gives

$$w(s + \Delta s) = w(s)\left(1 - \ell_c^{-1}\Delta s\right) + \sqrt{2\ell_c^{-1}\Delta s}\zeta(s), \tag{A2}$$

where $\zeta(s)$ denotes a Gaussian random variable with zero mean and unit variance. The discretization Δs is chosen much smaller than ℓ_c. Here we set $\Delta s = 10^{-2}\ell_c$.

Step 3: Propagation of particle position and time The particle positions are incremented at each random walk step by $\Delta s/\chi$, the particle times by $\Delta s/v_\ell(s)$,

$$x(s + \Delta s) = x(s) + \frac{\Delta s}{\chi}, \qquad t(s + \Delta s) = t(s) + \frac{\Delta s}{v_\ell(s)}. \tag{A3}$$

The current particle speed $v_\ell(s)$ is obtained according to Eq. (7).

Steps 2 and 3 are repeated until the maximum simulation time is reached. Particle positions are recorded at steps s if $t(s) \leq t_i$ and $t(s + \Delta s) > t_i$ with t_i the desired observation times.

Appendix B: Plume prediction for extended initial distribution

Figure 5 shows the predictions of the upscaled model for pointlike and extended initial particle distribution. The differences between the two predictions are very small, which confirms the robustness of the model, and the physical systems regarding the initial particle distribution. In general, the extended initial distribution, gives a better prediction of the data at $x = -5$ m, and a slightly better prediction of the maximum concentration at $x = 5$ m. At larger distances, the predicted concentration values are essentially identical.

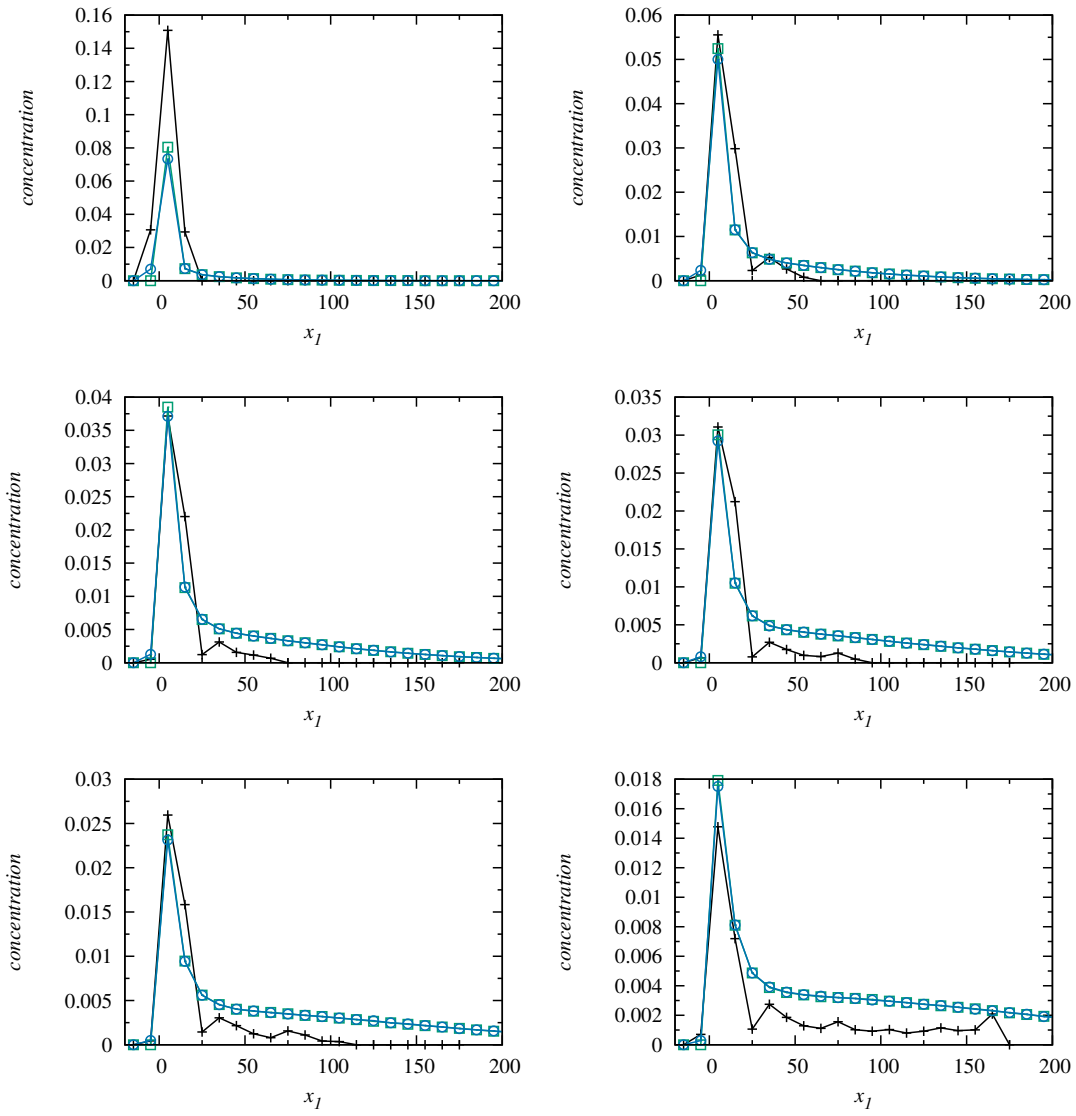

Figure 5. Concentration profiles from the (black crosses) MADE data, and the upscaled model for an averaging window of $\Delta x = 10$ m with (green squares) pointlike initial condition and (blue circles) uniform initial condition of extension 2.64 m centered in $x = 0$, at times (top left to bottom right) $t = 49$ d, 126 d, 202 d, 279 d, 370 d and 503 d.